KSME

Springer

Journal of Mechanical Science and Technology 35 (2) 2021

Original Article
DOI 10.1007/s12206-021-0115-1

Keywords:
· Boattail angle
· Base drag
· Boattail pressure drag
· Free-levitation test

Correspondence to:
The Hung Tran
thehungmfti@gmail.com

Citation:
Tran, T. H., Dinh, H. Q., Chu, H. Q., Duong, V. Q., Pham, C., Do, V. M. (2021). Effect of boattail angle on near-wake flow and drag of axisymmetric models: a numerical approach. Journal of Mechanical Science and Technology 35 (2) (2021) 563~573.
http://doi.org/10.1007/s12206-021-0115-1

Received February 27th, 2020
Revised September 28th, 2020
Accepted October 19th, 2020

† Recommended by Editor
Yang Na

Effect of boattail angle on near-wake flow and drag of axisymmetric models: a numerical approach

The Hung Tran[1], Hoang Quan Dinh[1], Hoang Quan Chu[1], Van Quang Duong[1], Chung Pham[1] and Van Minh Do[2]

[1]Faculty of Aerospace Engineering, Le Quy Don Technical University, 236 Hoang Quoc Viet, Bac Tu Liem, Hanoi, Vietnam, [2]Faculty of Special Equipments, Le Quy Don Technical University, 236 Hoang Quoc Viet, Bac Tu Liem, Hanoi, Vietnam

Abstract Flow behavior around axisymmetric boattail surface was studied by numerical methods. A wide range of boattail angles from 0° to 24° was investigated to find the drag trend of the model. Numerical simulation was validated by experimental results with the same flow conditions. Results showed that the use of boattail model always has a positive effect on drag reduction. Total drag showed minimum value at boattail model of around 14°. Length of the recirculation after body decreases with increasing boattail angle up to 14° and then becomes constant at higher angle. The trend of boattail pressure drag showed similar to previous studies for high-speed flow. However, base drag showed different trend to previous observation. The base drag showed to be the most important parameter to determine drag trend of the model. The effect of flow fields around boattail on pressure distribution and drag is discussed in detail.

1. Introduction

A boattail model added to an axisymmetric blunt-based body is a well-known device for drag reduction. The main advantages of boattail are that it modifies the flow structure of the near-wake by reducing recirculation length and turbulent intensity [1-4]. Consequently, the base pressure increases and the base drag decreases. However, the flow structure around boattail model is sufficiently complicated. Clearly, drag reduction depends on boattail parameters, which include its length, angle and shape of conjunction between boattail and main body.

Many studies have been conducted at high-speed conditions to understand effect of boattail model on drag reduction [5-8]. The boattail device was successfully applied for different flying objects, such as cargo airplanes, missile and projectile. The optimal boattail angle was found at around 7.9° with a length of 1.0 body diameter at high-speed conditions [9]. At angle higher than 7.9°, separation flow occurs near the conjunction and the boattail is inside the wake region. Additionally, the existence of shock wave near the conjunction leads to an increase in aerodynamic drag.

Although many studies have been conducted on high-speed flow, studies of near-wake flow at low-speed conditions are still limited. The lack of shock wake and compressible effects could lead to a significant difference in flow behavior in those cases. Lavrukhin and Popovich [10], for example, predicted that the angle where flow on boattail surface changes to fully separation conditions increases when the Mach number decreases. Consequently, boattail angle with minimum drag is higher at subsonic conditions. Suliman et al. [11], who conducted numerical simulation for boattail model of two-dimensional flow at Mach number of around 0.7, indicated that the optimal boattail angle is around 14°-16°. However, flow fields on the boattail surface were not analyzed in their studies. Recently, Mariotti et al. [12] conducted experiments to evaluate the effect of boattail on wake structure and drag reduction of the model. Differing from previous studies, drag of boattail model in their study monotonically decreases with increasing boattail angle up to 40.3°, where separated flow occurs on the boattail surface. Additionally,

adding a groove cavity on boattail surface could lead to large change of flow on boattail surface and near-wake structure. Tran et al. [13], who conducted an experiment on conical boattail at low-speed condition, found that a separation bubble could exist on boattail surface and affect its pressure drag. Lately, Tran et al. [14] conducted free-levitated test to measure total drag and indicated that the boattail model of 14° showed lower drag by comparison to the case of 10° and 20°. However, since the experiment was limited by the measurement devices, only the main information for some boattail models was presented. Clearly, flow behavior on boattail surface and the near-wake structure should be considered for evaluating aerodynamic drag of the model. Additionally, a systematic investigation for a wide range of boattail model should be conducted to fully understand effect of boattail angle on drag reduction.

Recently, the development of computational technology has provided a powerful tool for analyzing fluid dynamics. Many turbulent models have been developed and showed high potential in analyzing flow. While Reynolds-averaged Navier-Stokes (RANS) equations could provide averaged flow behavior with saving numerical time, large eddy simulation (LES) and direct numerical simulation (DNS) schemes provide unsteady flow behavior. However, LES and DNS schemes require a high powerful computer system and high time-consuming. Generally, the RANS scheme could provide sufficiently accurate results for incompressible flow and is applied widely in research [15-17].

In this study, the effect of boattail angle on drag reduction and near-wake structure of axisymmetric body was investigated by numerical methods. For this arm, varied boattail models with the same length but different angle were studied. The *k-ω* shear stress transport (*k-ω* SST) turbulent model was used for numerical scheme to obtain highly accurate results on the boundary layer and to reduce the numerical time. The numerical results were compared to experimental data in free-levitated test with the same flow conditions for validation. Numerical results indicate that the flow on boattail surface shifts to fully separated condition at boattail angle of around 18°. Additionally, the base drag shows to be the most important parameter to determine drag trend of the axisymmetric model. Drag coefficient is minimum at boattail model of around 14°-16°, which corresponds to maximum base pressure. Moreover, the boattail pressure drag increases with boattail angle, while the afterbody drag shows the same trend with base drag of the model. The relation between flow fields around boattail and drag of model will be discussed in detail in this study.

2. Numerical methods

2.1 Model geometry and numerical conditions

The axisymmetric models used in this study are the same as the one in the previous experimental study by Tran et al. [13]. The models have a diameter of D = 30 mm and a total length of L = 251 mm. The front part of the model has ellipsoid shape

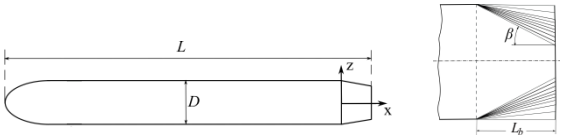

(a) Axisymmetric model (b) Zoom-in boattail

Fig. 1. Model geometry.

to avoid separation flow on the surface. The boattails have a conical shape with different angles β ranging from 0° to 24°. A total of eleven boattail models were used for this study. The length of boattail L_b is fixed at 0.7D (Fig. 1).

The numerical domain has a size of 33D×5D×5D, which has the same size of test section to the case of the experimental method. Since the model does not create lift and studies mainly focus on near-wake region, the selection of computational domain is sufficient for steady results.

An inlet velocity of U_∞ = 22 m/s was imposed on the inflow plane, which is located at 7D before the nose of model. Note that the selected velocity in this study is similar to the velocity of most road tankers on the highway. Additionally, we selected velocity the same as the experiments in previous studies [13, 14]. Consequently, the results of the study could be validated and compared. Slight increase of velocity has little effect on flow pattern and drag except at critical angle where the flow is shifted to fully separated condition. Since this study focuses on wake of the model by numerical approach, we did not investigate the effect of Reynolds number on flow pattern.

The Reynolds number based on the diameter of the model is $Re = 4.34\times10^4$. On the side boundaries of numerical domain, symmetric conditions were used.

2.2. Numerical scheme and mesh generation

k-ω SST turbulent model was selected to obtain averaged flow fields around the model. *k-ω* SST model is mixed between *k-ω* model for flow near the wall and *k-ε* model for flow far from the wall. The selection of *k-ω* model allows obtaining highly precise results near the surface while it also reduces the numerical time. The model was used widely in previous studies for fluid flow [18-21]. Note that flow on boundary layer of boattail will affect pressure distribution and drag of the model. Consequently, *k-ω* SST model was used in this study to obtain a precise boundary layer profile.

We used commercial software ANSYS FLUENT Version 12.1, which was copyrighted by Faculty of Aerospace Engineering, Le Quy Don Technical University, Hanoi, Vietnam for computational scheme. *k-ω* SST model is based on RANS equations with additional two eddy-viscosity equations for turbulent kinetic energy k and specific dissipation rate ω. In detail, the RANS model is written as the following:

$$\frac{\partial \rho}{\partial t}+\frac{\partial}{\partial x_i}(\rho u_i)=0 \tag{1}$$

$$\frac{\partial}{\partial t}(\rho u_i)+\frac{\partial}{\partial x_j}(\rho u_i u_j) = -\frac{\partial p}{\partial x_i}+\mu\frac{\partial}{\partial x_j}\left(\frac{\partial u_i}{\partial x_j}+\frac{\partial u_j}{\partial x_i}\right)+\frac{\partial}{\partial x_j}\left(-\rho\overline{u_i'u_j'}\right) \quad (2)$$

where i, j = 1, 2, 3; u_i is averaged velocity component, p is pressure, ρ is air density and σ_{ij} is stress tensor component; $-\rho\overline{u_i'u_j'}$ is the Reynolds shear-stress term.

The equations for k and ω are as [22]:

$$\frac{\partial(\rho k)}{\partial t}+\frac{\partial(\rho u_j k)}{\partial x_j} = P+\beta^*\rho\omega k+\frac{\partial}{\partial x_j}\left[(\mu+\sigma_k\mu_t)\frac{\partial k}{\partial x_j}\right] \quad (3)$$

$$\frac{\partial(\rho\omega)}{\partial t}+\frac{\partial(\rho u_j\omega)}{\partial x_j} = \frac{\gamma}{\nu_t}P-\beta\rho\omega^2 +\frac{\partial}{\partial x_j}\left[(\mu+\sigma_k\mu_t)\frac{\partial\omega}{\partial x_j}\right]+2(1-F_1)\frac{\rho\sigma_{\omega 2}}{\omega}\frac{\partial k}{\partial x_j}\frac{\partial\omega}{\partial x_j} \quad (4)$$

where ν_t is eddy-viscosity and is defined as:

$$\nu_t = \frac{a_1 k}{\max(a_1\omega;\Omega F_2)} \quad (5)$$

In those equations, σ_k, $\sigma_{\omega 2}$, β, β^*, κ, γ are constant parameters and are selected two times for flow near the surface and flow far from the surface of the model. For the detailed information of parameters in Eqs. (3)-(5), readers can refer to Menter [22, 23].

The computation domain was divided into small blocks and was meshed by hexahedron structure cells. The mesh around the model is presented in Fig. 2. The first layer on the model surface has a height of 0.008 mm, which corresponds to $y^+ < 1$ (Fig. 3). The increasing ratio above the model surface is 1.055, which ensures that the boundary layer is captured well in this study.

The SIMPLE algorithm was applied to find the pressure and velocity fields. This study used different structured grid sizes of 1.2 million, 2.8 million, 4.8 million and 6.5 million cells to check the grid sensitivity. The drag coefficient was tested for boattail model of 14° for different grid sizes. The results are shown in Fig. 4. Clearly, the drag coefficient changes slightly at different mesh size and it converges for cell number higher 2.8 million. The mesh with 4.8 million cells was selected for this study for accurate results and saving numerical time.

2.3 Boattail pressure drag and base drag calculations

The numerical results allow one to calculate each components drag of the model. The pressure drags of the model are

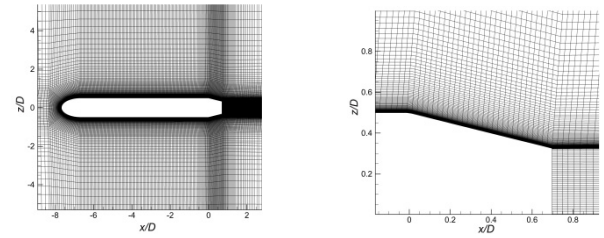

(a) Structure of mesh around model (b) Structure of mesh around boattail

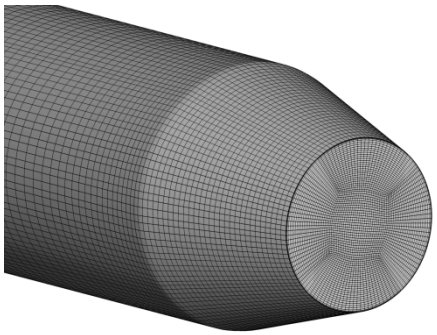

(c) Mesh on the boattail surface

Fig. 2. Mesh around the model.

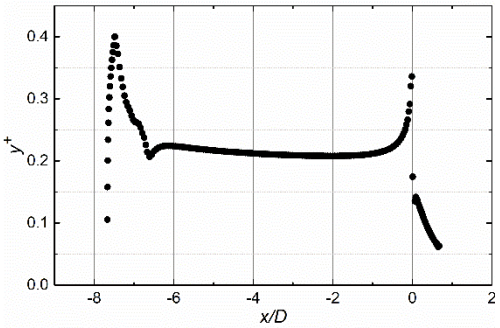

Fig. 3. y-plus on the wall of model.

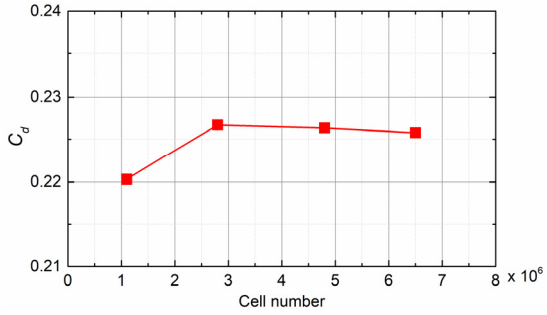

Fig. 4. Effect of cell number on drag of model.

calculated by the below equations:

$$C_{Dp,\beta} = \frac{1}{R^2}\int_{R^2}^{r_b^2} C_{P,\beta}(x)\,dr_x^2 \quad (6)$$

$$C_{Dp,b} = \frac{-r_b^2}{R^2}\bar{C}_{P,b} \quad (7)$$

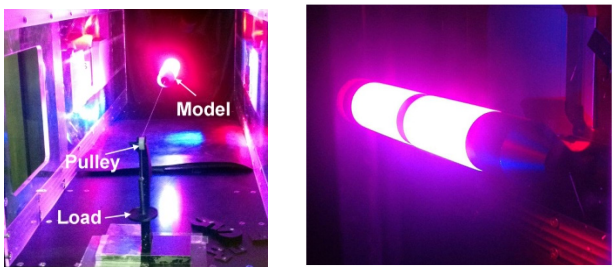

(a) Model in calibration process [14] (b) Model in free levitation

Fig. 5. Mode in calibration and free-levitated test.

where $C_{Dp,\beta}$, $C_{Dp,b}$ are boattail pressure drag and base drag, respectively. R is the diameter of the model, r_b is base diameter, r_x is radius of boattail at x position. $C_{P,\beta}(x)$ is pressure at x position on the top symmetric surface of boattail model and $\overline{C}_{P,b}$ is mean pressure value on the base surface.

3. Experimental setup

The main feature of the experimental setup, which was conducted in previous study by Tran et al. [14], is now recalled to validate the numerical results. The experiment was conducted to measure total drag force measurement of the model at different boattail angles. The experiment used the magnetic suspension and balance system (MSBS) at Department of Aerospace Engineering, Tohoku University, Japan. The system allows levitating a model freely in a wind tunnel using magnetic force. In detail, a permanent magnet is inserted inside the model. Additionally, ten electric magnets are inserted around the test section. The interaction between permanence magnet and electric magnetic fields allows one to control the positions and attitude of the model. Since the model is free-levitated, the effect of support system on drag measurement does not occur. The detailed structure and working principle of the system were presented by Sawada and Suda [24].

The model in free-levitated test is presented in Fig. 5. Since the setup of the experiment is sufficiently complicated and time consuming, only three boattail models of 10°, 14° and 20° were investigated (see Ref. [14]). The velocity of the wind tunnel was fixed at 22 m/s, which is the same as the numerical method.

For measuring total drag, a drag force calibration process is required. The purpose of the process is to obtain the relation between the force acting on the model and current of the coil. After that, the change of current during wind tunnel test is transferred to force from the calibration data. The details of the calibration process were presented by Tran et al. [14]. To avoid hysteresis of the magnet, the calibration process was repeated six times and mean value was calculated. Results of the calibration process show high linear dependence between the force acting on the model and the current coil (Fig. 6). Consequently, the calibration data can be applied for measuring static drag force of the model.

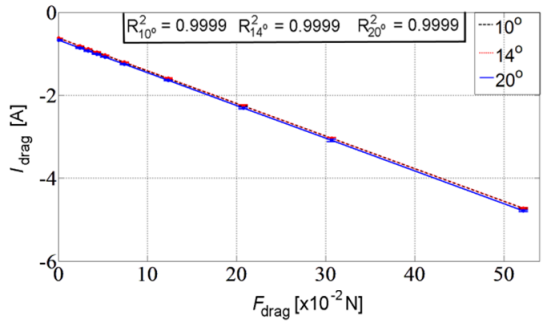

Fig. 6. Calibration results on magnetic suspension and balance system [14].

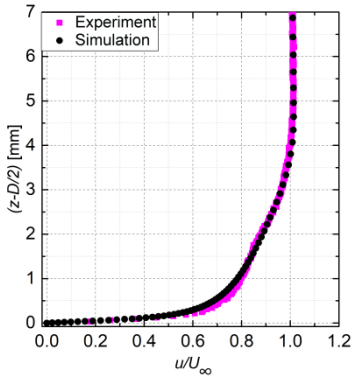

Fig. 7. Boundary layer profile on boattail model at β = 16°.

4. Results and discussion

4.1 Validation of numerical results

Fig. 7 shows the boundary layer profiles 6 mm before the conjunction (x/L_b = -0.12) by numerical method for boattail model of 16°. The experimental results of Tran et al. [24] using particle image velocimetry were also added. By choosing small heights of the mesh near the surface, we obtained a detailed boundary layer profile. Additionally, the numerical results show close results to the experimental method. Note that the model in the numerical method did not use tripping wire to create turbulent boundary layer as in the case of experiments. Clearly, with the initial flow conditions and geometrical parameters of the models, the boundary layer is shifted to turbulent before the boattail conjunction. The simulation provides sufficiently accurate results, which could be used for further discussion.

Table 1 shows parameters of boundary layer by numerical approach, which include displacement thickness δ^*, momentum thickness θ and H-factor. The H-factor is around 1.6, which indicates that the boundary layer close to the conjunction is fully turbulent.

Fig. 8 presents pressure distribution on the boattail surface for the case of β = 16°. The experimental results were by Tran et al. [25] at the same boattail model and two velocities of U_∞ = 22 m/s and U_∞ = 45 m/s. The numerical results show clear results to experimental data on the boattail surface, except near the conjunction. It is believed that the airflow in numerical

Table 1. Characteristics of boundary layer.

Parameters	Value
δ_{99}/D	0.227
δ^*/D	0.0490
θ/D	0.0357
H-factor	1.60

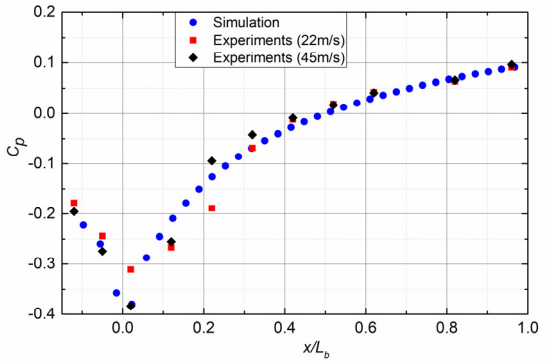

Fig. 8. Pressure distributions on boattail surface by experiments and numerical methods.

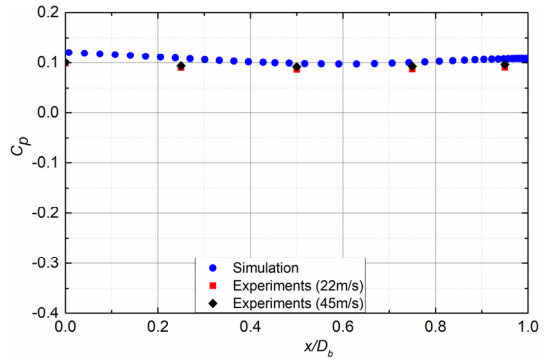

Fig. 9. Pressure distribution on base surface by experiments and numerical methods.

method is highly ideal and it cannot simulate the flow phenomenon near the conjunction. On the other hand, the separation bubble at low-speed condition affects pressure distribution near the conjunction and it leads to some different results by comparison to numerical methods. However, since the boattail is sufficiently long, the separation bubble has practically no effect on boattail pressure drag. Numerical results can thereby be used to obtain general information about aerodynamic drag of the model.

The pressure distribution on the base surfaces is in high agreement for both experiments and numerical methods. The pressure at the base changes slightly along the radius and can be considered as a constant value on the whole base. Additionally, the results show that the difference of pressure between numerical and experimental methods is less than 7 % (Fig. 9).

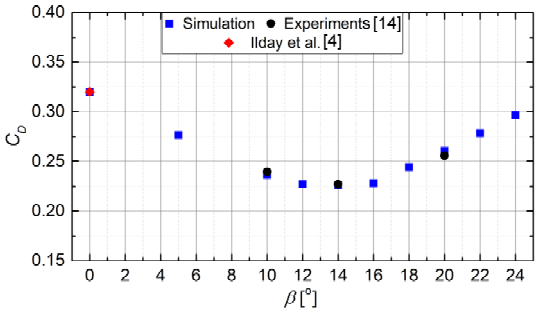

Fig. 10. Drag of model at different boattail angles.

4.2 Drag of the model

The drag coefficient of the models by numerical scheme and by the free-levitated test is shown in Fig. 10 for different boattail angles. The drag measurement in free-levitated test was conducted for three boattail models of 10°, 14° and 20°. Additionally, the drag coefficient of blunt-based body (β = 0°), which was presented in previous study by Ilday et al. [4], is also plotted. Results indicate that the different drag coefficient between numerical and experimental methods is less than 5 %. Interestingly, using boattail model between 5° to 24° decreases drag of model. Additionally, minimum drag exists at a boattail angle around 14°, where drag is reduced around 40 % by comparison to the blunt-based model. The decreasing drag of model when boattail angle increases from β = 0° to β = 14° can be explained by reducing near-wake structure and turbulent intensity after the body. However, to analyze drag trend at boattail angles higher than 14°, the flow behavior around the boattail should be analyzed.

The existence of minimum drag was well noted in previous studies for high subsonic and supersonic flow. However, compared to supersonic conditions where minimum drag occurs at angle of around 7.9° [6], the boattail model obtains minimum drag at much higher boattail angle. The existence of a shock wave near the conjunction is the main factor, which leads to different angle of minimum drag at supersonic conditions by comparison to the low-speed conditions. Clearly, the flow phenomenon on boattail surface is a very important parameter that affects pressure distribution and drag of models at low-speed conditions.

However, the drag trend in this study shows different from the one in previous studies by Buresti et al. [26] and Mariotti et al. [12] for contour boattails, where drag coefficient decreases with increasing boattail model up to 40.3° and the model with minimum drag was not reported. The difference of conjunction shape is probably a factor affecting results. The existence of minimum drag for axisymmetric boattail angle at incompressible flow is quite interesting, which is first presented in this study. The differences in boattail shape, flow condition and Reynolds number are probably factors affecting drag trend of the model. For understanding this phenomenon, flow behavior on the boattail surface and each components of pressure drag should be analyzed.

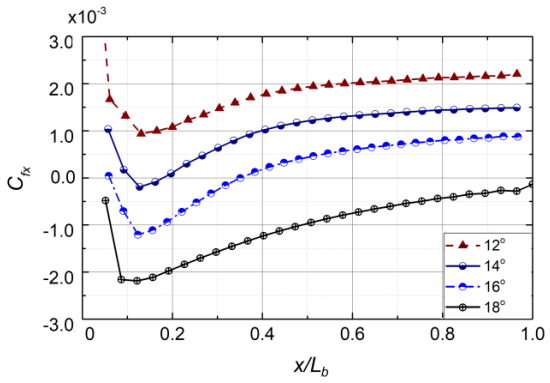

Fig. 11. Skin-friction on boattail surface.

4.3 Skin-friction coefficient and separated flow on boattail surface

Separation flow on the boattail surface could be determined by analyzing streamwise skin-friction distribution on the surface. In the details, separation position is determined by a position where skin friction changes from positive to negative while the reattachment position is determined by a position where the value changes from negative to positive. The method was presented in previous study by Lee et al. [27] for flow on airfoil by numerical methods. In our study, streamwise skin-friction coefficient is calculated by the following equation:

$$C_{fx} = \frac{\mu}{q}\left(\frac{du}{dz}\right)_{z=0} \tag{8}$$

where C_{fx} is skin-friction coefficient in x direction, μ is viscosity coefficient and q is dynamic pressure.

Fig. 11 shows skin-friction values on the boattail surface for the angle from 12° to 18°, which presented the most important three features of flow fields on the boattail. At boattail angle of 12°, the flow is attached on boattail surface. However, at boattail model of 18º, the flow separates on the whole boattail surface characterized by the region of negative skin friction. For the boattail angle between 12° to 18°, a separation bubble occurs near the conjunction of the model. The length of separation bubble increases with boattail angle and reaches around 35 % of total boattail length at β = 16º. The existence of separation bubble region on boattail surface at low-speed condition differs from the case of supersonic flow, where only two flow types were observed [10, 28]. Three flow types were observed on the boattail surface by numerical method, and transition regime is at boattail angles between 12° and 18°.

The existence of the separation bubble on the boattail surface was similar to the previous experimental study by Tran et al. [13]. However, since RANS provides only averaged results and the conjunction of boattail model is perfectly smooth, we cannot observe clearly results as shown by experimental data. In those cases, other numerical schemes, such as LES of DNS with high resolution of mesh, should be conducted and the effect of conjunction shape between boattail and main body should be investigated. Note that the separation bubble on boattail mainly has an effect on drag at critical boattail angle. Since this study focuses on near-wake flow and drag of the model, the results are sufficient for the discussion.

4.4 Averaged flow fields around the model

Averaged flow fields on symmetric plane around the boattail models are shown in Fig. 12. Here the x and z axes are normalized by diameter of the model. Clearly, flow accelerates above the boattail conjunction and velocity is higher than free-stream velocity. The effect can be observed for all boattail configurations. It leads to the development of boundary layer thickness and decreases of pressure around the conjunction.

Fig. 12 also shows that the near-wake flow region becomes narrower with increasing boattail angles to around 16°. At boattail model of 18°, separation flow occurs at the conjunction and the flow around the boattail surface at that angle is characterized by two vortexes: a small one on the boattail surface and a large one after the surface. However, at that angle, the vortex flow on the boattail surface is small. As the boattail angle increases, the vortex on the boattail surface becomes larger and the center of the vortex moves downstream. When the boattail model reaches 24°, the separated flow on the boattail surface is mixed with near-wake flow to form a large wake region around the boattail. The flow behavior could lead to a significant change of pressure distribution on the boattail model and increase the drag of the model.

Fig. 13 presents the position of the main vortex center after body for fully-separated flow at boattail angles between 18° and 24°. Interestingly, the center of vortex moves upstream when the boattail angle increases. The effect is different from flow on slant surface of Ahmed body, where the recirculation flow becomes larger and the main vortex center moves downstream as the slant angle increases [29]. It can be explained that the separation bubble develops on surface with increasing boattail angle and it becomes a significant feature at a critical angle. Additionally, the wake of the axisymmetric model is not as strong as the case of two-dimensional flow. Consequently, the interaction of separation bubble on the surface and recirculation region leads to move upstream of main vortex. Additionally, the effect of Reynolds number is also another factor leading to the different results.

4.5 Velocity at centerline and length of recirculation after body

The streamwise velocity at centerline of the near-wake flow is shown in Fig. 14 for different boattail angles from 0° to 24°. Clearly, the maximum velocity magnitude inside the near-wake region decreases quickly with increasing boattail angle up to 16°. For the blunt-based body, the maximum velocity in the reversed region reaches around 0.4 of free-stream velocity, which is highly consistent with the previous result by Merz et al.

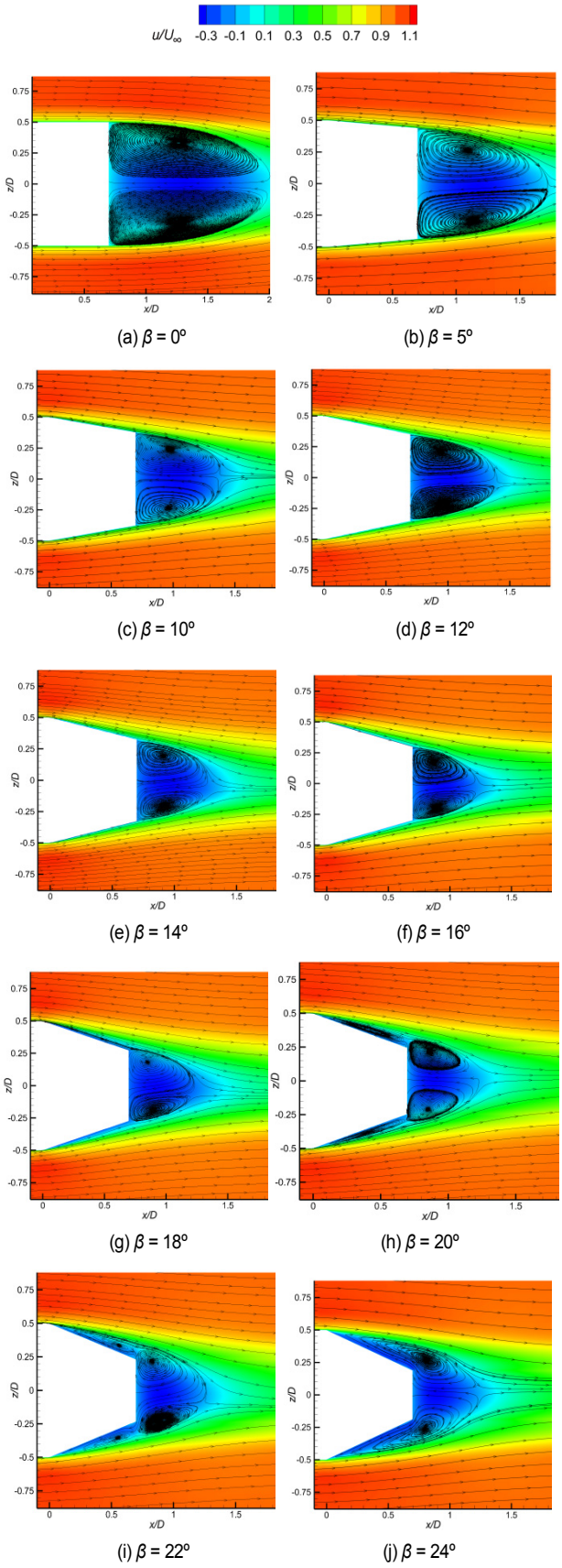

Fig. 12. Streamlines flow over boattail surface at different angles.

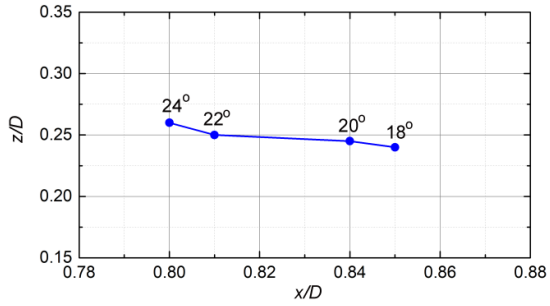

Fig. 13. Position of main vortex center for boattail angles from 18° to 24°.

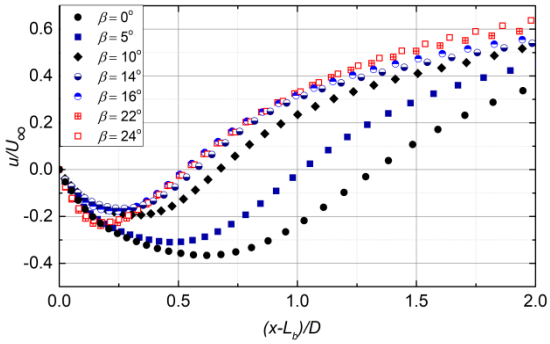

Fig. 14. Velocity at centerline for different boattail angles.

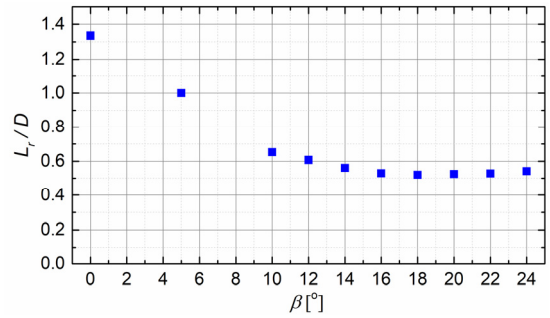

Fig. 15. Length of recirculation at different boattail angle.

[30]. At boattail model of 16°, velocity magnitude in reversed flow region is around 0.18 of free-stream velocity. The model with minimum drag is connected with the minimum magnitude of velocity inside the wake region. Interestingly, although drag coefficient at boattail model of 24° is higher than the case of 5°, the maximum magnitude of velocity inside the wake region at β = 24° is smaller than that of β = 5°.

Fig. 15 summarizes the length of the recirculation region for different boattail angles. The length of the recirculation is determined by a distance from the base to a point after body, where the velocity on the centerline changes from negative to positive. At boattail model of 0°, the length of recirculation region is around 1.3*D*, which is highly consistent with previous studies [31, 32] for similar Reynolds number. The length of recirculation decreases quickly when boattail angle increases from 0° to 10°. However, for boattail model higher than 10°, the length of recirculation changes slightly at different boattail con-

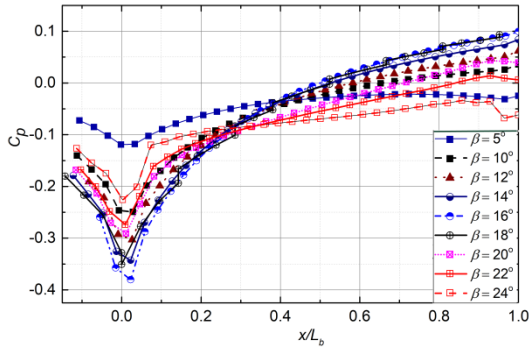

Fig. 16. Pressure distribution on boattail surface for different boattail configuration.

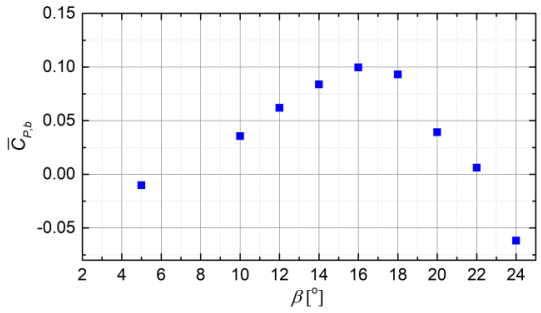

Fig. 17. Averaged base pressure as function of boattail angles.

figurations. At boattail angle greater than 20°, the length of the recirculation region slightly increases again, which corresponds to the widening wake region. Interestingly, the length of recirculation region does not change much at boattail angle above 14°. The fully-separated flow may lead to lower streamwise velocity inside the recirculation region, as was shown in Fig. 14. Consequently, the length of recirculation region is not the main factor which affects the drag trend of the model. In fact, pressure distribution on boattail and base surface should be analyzed.

4.6 Pressure distribution on boattail and base surfaces

In this section, we analyze pressure distribution on boattail and base surfaces to understand the effect of boattail angle on drag of the model. As shown in Sec. 4.1, pressure trend by numerical simulation is close to the case of experimental method for the case of 16°, which indicates that numerical simulation provides sufficient results for the discussion. Here, pressure distribution on boattail surface for different angle is presented in Fig. 16. Since the model is symmetric, only pressure values on the top surface of the symmetric plane are selected. Clearly, the existence of boattail increases velocity above the boundary layer, which results in the low-pressure region near the conjunction. Pressure recovers quickly again after the conjunction. The effect of boattail angle on the peak of pressure near the conjunction is large for boattail angle below 18°. However, when the flow is fully separated, pressure is redistributed on the boattail surface. In detail, the movement of vortexes around the boattail leads to a lower pressure peak and widens the low-pressure region. The distribution of pressure around the base edge showed a similar trend to previous observation in subsonic condition by Chamberlin and Blaha [33] where separation flow is characterized by low-pressure region while the attached flow is characterized by high pressure around the base edge.

However, the change of pressure near the conjunction with increasing boattail angle shows different trend to the case of high-speed condition, where the peaks of pressure become lower at higher boattail angles [28]. It can be explained that the pressure distribution on boattail surface at low-speed conditions is affected by flow behavior while pressure distribution at high-speed conditions is mainly affected by the geometry of the model.

The mean value of the base pressure coefficient at different boattail angles is shown in Fig. 17. The maximum base pressure occurs at a boattail angle around 16°, which corresponds to the change of main separation position. As the separation moves to the conjunction, the base pressure decreases.

When boattail angle increases from 18° to 24°, the movements of the vortex on boattail surface and the main vortex of the wake result in dramatic decrease of base pressure. Clearly, we observed that the base pressure does not depend mainly on the length of recirculation, which generally is observed for supersonic flow [8]. Additionally, the base pressure does not monotonically decrease with increasing boattail angle, which was generally observed in a previous study [26].

4.7 Boattail pressure drag and base drag

The pressure distribution on boattail and base surface allows one to calculate boattail pressure drag and base drag of the model. Here, Eqs. (6) and (7) in Sec. 2.4 were applied. Fig. 18 shows the results of boattail pressure drag, base drag and afterbody pressure drag for different boattail angles. Overall, boattail pressure drag increases with boattail angle from 5° to 24°, while base drag shows a minimum value at boattail angle around 16°. The afterbody pressure drag as the sum of boattail pressure drag and base drag shows the same trend to base drag with a minimum value around boattail model of 14°. Clearly, base drag is the most important parameter to determine the drag trend of axisymmetric boattail model at low-speed conditions.

The trend of boattail pressure drag shows similar features to previous studies for contour boattail angles [12] and for supersonic flow [6, 28]. However, base drag shows a different trend to previous observations at supersonic flow where base pressure monotonous decreases with increasing boattail angle [8]. Consequently, the minimum drag at supersonic flow occurs from different trend of boattail pressure drag and base drag.

In this study, we used an axisymmetric model with boattail

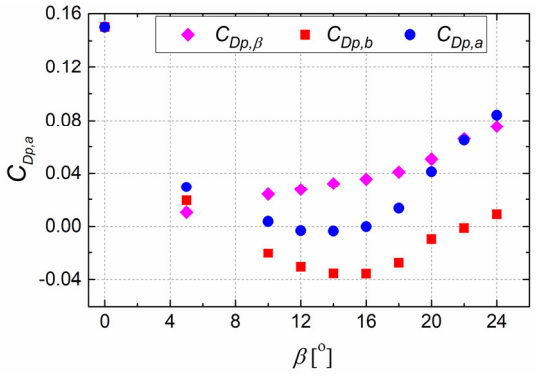

Fig. 18. Pressure drags of different boattail angles.

length of 0.7*D*. At other parameters of boattail length, the base area was changed. Consequently, it will be affecting base drag values as shown in Eq. (7). Interestingly, Figs. 17 and 18 indicate that the mean base pressure and base drag show the same extreme point at boattail angle around 16°. Consequently, it is believed that the minimum drag exists for different boattail lengths at low-speed conditions.

5. Conclusions

The effect of boattail angle on the drag of axisymmetric model was investigated at low-speed conditions. A wide range of boattail model was tested. Both experimental and numerical methods were applied for measuring drag of the model. Numerical simulation by *k-ω* SST model showed close results to experimental data. The main conclusions of the paper are as follow:

There is a boattail angle at around 14°, where drag of the model obtains minimum value at low-speed conditions. The boattail angle with minimum drag at low-speed flow is much higher than the case of high-speed conditions and was first presented in this study.

Boattail model has high effect on drag reduction, even when the flow is fully separated on the boattail surface. When the flow is fully separated, increasing boattail angle leads to increase of aerodynamic drag.

The peak of pressure near the conjunction becomes lower when boattail angle increases to 18°. However, the fully separated flow leads to redistributing pressure on the boattail surface with widening low-pressure region.

Length of recirculation after body decreases with increasing boattail angle up to 14° and then it is almost constant with increasing boattail angle.

Boattail pressure drag shows an upward trend with increasing boattail angle. Base drag decreases with increasing boattail angle to 16° and then it increases again. When the flow is fully separated near the shoulder ($\beta \geq 18^{o}$), the main parameters' effect on base drag is the movement of vortexes after body. Base drag is the most important parameter to determine drag trend of axisymmetric boattail model at low speed.

Acknowledgments

The authors thank Professor Keisuke Asai and Professor Taku Nonomura at Department of Aerospace Engineering, Tohoku University in Japan for their support during the experimental process.

References

[1] W. A. Mair, Reduction of base drag by boat-tailed afterbodies in low speed flow, *Aeronautical Quanterly*, 20 (1969) 307-320.

[2] W. A. Mair, Drag-reducing techniques for axisymmetric bluff bodies, *Proceedings on the Symposium on Aerodynamic Drag Mechanisms of Bluff Bodies and Road Vehicles,* Edited by Sovran, G., Morel, T., Mason, W. T., General Motors Research Laboratories, Plenum Press, New York (1978) 161-178.

[3] F. G. Howard and W. L. Goodman, Axisymmetric bluff-body drag reduction through geometrical modification, *J. of Aircraft*, 20 (6) (1985) 516-522.

[4] O. Ilday, H. Acar, M. K. Elbay and V. Atli, Wakes of three axisymmetric bodies at zero angle of attack, *AIAA J.*, 31 (6) (1992) 1152-1154.

[5] D. E. Reubush, Effect of reynolds number on boattail drag, *J. of Aircraft*, 13 (5) (1976) 334-337.

[6] M. Tanner, Steady base flows, *Progress in Aerospace Sciences*, 21 (1984) 81-157.

[7] P. R. Viswanath, Flow management techniques for base and fterbody drag reduction, *Progress in Aerospace Sciences*, 32 (1991) 79-129.

[8] R. M. Cummings, H. T. Yang and Y. H. Oh, Supersonic, turbulent flow computation and drag optimization for axisymmetric afterbodies, *Computers and Fluids*, 24 (4) (1994) 487-507.

[9] R. J. Krieger and S. R. Vukelich, Tactical missile drag, tactical missile aerodynamics, *Prog. Astronautics Aeronautics, AIAA J.*, 104 (1986) 383-420.

[10] G. N. Lavrukhin and K. F. Popovich, *Aero-gas-dynamics of Jet Nozzles, Volume 2. Flow around the Base*, Fizmatlit Moscow Russia (in Russian) (2009).

[11] M. A. Suliman, O. K. Mahmoud, M. A. Al-Sanabawy and O. E. Abdel-Hamid, Computational investigation of base drag reduction for a projectile at different flight regimes, *13th International Conference on Aerospace Sciences and Aviation Technology*, Cairo, Egypt, ASAT-13-FM-05, May 24-26 (2009).

[12] A. Mariotti, G. Buresti, G. Gaggini and M. V. Salvetti, Separation control and drag reduction for boat-tailed axisymmetric bodies through contoured transverse grooves, *J. of Fluid Mechanics*, 832 (2017) 514-549.

[13] T. H. Tran, T. Ambo, T. Lee, L. Chen, T. Nonomura and K. Asai, Effect of boattail angles on the flow pattern on an axisymmetric afterbody at low speed, *Experimental Thermal and Fluid Science*, 99 (2018) 324-335.

[14] T. H. Tran, T. Ambo, L. Chen, T. Nonomura and K. Asai, Effect of boattail angle on pressure distribution and drag of axisymmetric afterbodies under low-speed conditions, *Transactions of the Japan Society for Aeronautical and Space Sci-*

ences, 62 (4) (2019) 219-226.
[15] D. Hertwig, G. C. Efthimiou, J. G. Bartzis and B. Leitl, CFD-RANS model validation of turbulent flow in a semi-idealized urban canopy, *J. of Wind Engineering and Industrial Aerodynamics*, 111 (2012) 61-72.
[16] K. Rogowki, Numerical studies on two turbulence models and a laminar model for aerodynamics of a vertical-axis wind turbine, *J. of Mechanical Science and Technology*, 32 (2018) 2079-2088.
[17] K. Rusin, W. Wróblewski and S. Rulik, The evaluation of numerical methods for determining the efficiency of Tesla turbine operation, *J. of Mechanical Science and Technology*, 32 (2018) 5711-5721.
[18] Y. J. An and B. R. Shin, Numerical investigation of suction vortices behavior in centrifugal pump, *J. of Mechanical Science and Technology*, 25 (2011) 767-772.
[19] N. Ashton, A. West, S. Lardeau and A Revell, Assessment of RANS and DES methods for realistic automotive models, *Computers and Fluids*, 128 (2016) 1-15.
[20] L. Zheng, X. Chen, H. S. Dou, W. Zhang, Z. Zhu and X. Cheng, Effects of clearance flow on the characteristics of centrifugal pump under low flow rate, *J. of Mechanical Science and Technology*, 34 (2020) 189-200.
[21] Y. T. Lee and H. C. Lim, Effect of turbulent boundary layer on the surface pressure around trench cavities, *J. of Mechanical Science and Technology,* 27 (2013) 2673-2681.
[22] F. R. Menter, Zonal two equation k-ω turbulence models for aerodynamic flows, *AIAA Paper* (1993) 1993-2906.
[23] F. R. Menter, Two-equation Eddy-viscosity turbulence models for engineering applications, *AIAA J.*, 32 (8) (1994) 1598-1605.
[24] H. Sawada and S. Suda, Study on aerodynamic force acting on a sphere with and without boundary layer trips around the critical reynolds number with a magnetic suspension and balance system, *Experiments of Fluids*, 50 (2011) 271-284.
[25] T. H. Tran, T. Ambo, T. Lee, K. Ozawa, L. Chen, T. Nonomura and K. Asai, Effect of Reynolds number on flow behavior and pressure drag of axisymmetric conical boattails in low-speed conditions, *Experiments in Fluids*, 60 (3) (2019).
[26] G. Buresti, G. V. Iungo and G. Lombardi, Method for the drag reduction of bluff bodies and their application to heavy road-vehicles, *1st Interim Report Contract between CRF and DIA*, DDIA 2007-6 (2007).
[27] D. Lee, T. Nonomura, M. Anyoji, H. Aono, A. Oyama, K. Asai and K. Fujii, Mechanisms of surface pressure distribution within a laminar separation bubble at different Reynolds numbers, *Physics of Fluids*, 27 (2015) 023602.
[28] W. M. Presz and E. T. Pitkin, Flow separation over axisymmetric afterbody models, *J. of Aircraft*, 11 (11) (1974) 677-682.
[29] T. Tunay, B. Sahin and V. Ozbolat, Effects of rear slant angles on the flow characteristics of Ahmed body, *Experimental Thermal and Fluid Science,* 57 (2014) 165-176.
[30] R. A. Merz, R. H. Page and C. E. G. Przirembel, Subsonic axisymmetric near-wake studies, *AIAA J.,* 16 (7) (1978) 656-662.
[31] T. H. Tran and L. Chen, Optical-flow algorithm for near-wake analysis of axisymmetric blunt-based body at low-speed conditions, *J. of Fluids Engineering*, 142 (2020) 111504.
[32] T. H. Tran, The effect of boattail angles on the near-wake structure of axisymmetric afterbody models at low-speed condition, *International J. of Aerospace Engineering*, 2020 (2020) 7580174.
[33] R. Chamberlin and B. J. Blaha, Flight and wind tunnel investigation of the effects of Reynolds number on installed boattail drag at subsonic speeds, *AIAA Paper*, No 73-139 (1973).

The Hung Tran is a lecturer at Faculty of Aerospace Engineering, Le Quy Don Technical University, Hanoi, Vietnam. He received his Ph.D. in Experimental Aerodynamics at Tohoku University, Japan in 2019. His research interests are numerical simulation, optical-flow and wind tunnel experiments.

Hoang Quan Dinh is a lecturer at Faculty of Aerospace Engineering, Le Quy Don Technical University, Hanoi, Vietnam. He received his Ph.D. at Moscow institute of Physics and Technology, Russian Federation in 2017. His research interests are numerical simulation, scientific computing, aerodynamics, fly engineering and wind tunnel experiments.

Hoang Quan Chu is a lecturer at the Faculty of Aerospace Engineering, Le Quy Don Technical University, Hanoi, Vietnam. He received his Master's at ISAE SUPAERO, France in 2016. His research interests are aerodynamics, propulsion and fluid-structure interactions.

Van Quang Duong is a Doctoral researcher at Faculty of Aerospace Engineering, Le Quy Don Technical University, Hanoi, Viet Nam. He received his Master's at Le Quy Don Technical University in 2017. His research interests are aerodynamic, aeroelasticity and aircraft structural.

Chung Pham is a lecturer at Faculty of Aerospace Engineering, Le Quy Don Technical University, Hanoi, Vietnam. He received his Ph.D. at Moscow Aviation Institute, Russian in 2012. His research interests are numerical simulation, aircraft construction.

Van Minh Do is the lecturer at Faculty of Special Equipments, Le Quy Don Technical University, Hanoi, Vietnam. He received his Ph.D. in Engineering Sciences at National University of Science and Technology MISiS, Russia in 2015. His research interests are numerical simulation, high velocity impact dynamics.